Use of interface phonon-polaritons for the alloy determination in ZnO/(Zn,Mg)O multiple quantum wells

M. Montes Bajo, J. Tamayo-Arriola, N. Le Biavan, E. Martínez Castellano, D. Lefebvre, Maxime Hugues, J.-M. Chauveau, A. Hierro

Applied Surface Science 567 (2021) 150816

Contents lists available at ScienceDirect

Applied Surface Science

journal homepage: www.elsevier.com/locate/apsusc

Full Length Article

Use of interface phonon-polaritons for the alloy determination in ZnO/(Zn,Mg)O multiple quantum wells

M. Montes Bajo [a,*], J. Tamayo-Arriola [a], N. Le Biavan [b,1], E. Martínez Castellano [a], D. Lefebvre [b], M. Hugues [b], J.-M. Chauveau [b,2], A. Hierro [a]

[a] ISOM, Universidad Politécnica de Madrid, 28040 Madrid, Spain
[b] Université Côte d'Azur, CNRS, CRHEA, 06560 Valbonne, France

ARTICLE INFO

Keywords:
ZnO
Quantum wells
Reflectance spectroscopy
Alloy determination
Interface phonon polariton
Composition-dependent phonon frequency

ABSTRACT

A method based on infrared reflectance spectroscopy is presented by which the Mg content in ZnO/(Zn,Mg)O multiple quantum wells with very thin barriers can be determined. The method relies on the observation of interface phonon-polaritons which appear as sharp dips in the *p*-polarized reflectance spectra at oblique incidence near the longitudinal optical (LO)-phonon frequencies of both QW and barrier materials. By fitting the reflectance spectra to a dielectric function model, the LO phonon frequency of the (Zn,Mg)O barrier layers can be determined. The LO phonon frequency depends on the Mg content. Comparing to Mg content calibration via cathodoluminescence, a linear relationship between the reflectance dip frequency and the Mg content is obtained. The presented method serves as a rapid means to determine the Mg content on final structures with very thin (Zn,Mg)O layers -such as device structures- where alternative, destructive methods cannot be used.

1. Introduction

ZnO and its alloy (Zn,Mg)O feature a unique set of characteristics that make them excellent candidates for fundamental Physics studies as well as electronic and optoelectronic applications. Examples of the former are the demonstration in ZnO/(Zn,Mg)O heterostructures of the Quantum Hall Effect (QHE) [1], and the odd- and even-denominator fractional QHE [2,3], owing to the large 2-dimensional electron densities achievable, up to 3.7×10^{12} cm^{-2} [1]. Moreover, two-dimensional electron densities as large as 4×10^{13} cm^{-2} have been demonstrated in Ga-doped ZnO/$Zn_{0.7}Mg_{0.3}O$ quantum wells (QWs) [4]. In terms of optoelectronic applications, the ZnO family of materials are well-known wide-bandgap semiconductors with applications as transparent conductive oxide layers in photodetectors and solar cells [5] and plasmonics [6], as well as active materials for ultraviolet (UV) detectors [7]. The large exciton binding energy of around 60 meV in ZnO and its positive impact on the efficiency of radiative recombination of electrons and holes at room temperature makes ZnO and excellent active material in visible and UV light emitting devices. Lack of a reliable p-type doping has precluded the deployment of p-i-n light emitting devices based on this material, though, and remains a challenge for ZnO in this sort of applications [8]. However, since the bandgap of ZnO can be engineered by alloying with Mg, allowing the growth of ZnO/(Zn,Mg)O multiple QWs [7], there are good prospects of using intersubband transitions to develop unipolar infrared (IR) and THz devices [4,9–12], avoiding thus the use of the elusive p-type doping. The longitudinal optical (LO)-phonon energy of ZnO of approximately 73 meV (590 cm^{-1}) [13] makes it a promising candidate for room temperature light-emitting devices in the THz range, such as quantum cascade lasers (QCLs) [12,14]. Moreover, the high control achieved in the growth of these ZnO/(Zn,Mg)O QWs has recently yielded the demonstration of a negative refractive index hyperbolic metamaterial based on ZnO [15].

Devices based on ZnO and its related alloys, as happens with most semiconductors, often consist of a stack of many thin layers with varying composition forming heterostructures such as multiple quantum wells (MQWs), superlattices, Bragg reflectors, or even much more intricate structures as QCLs, to name a few. Knowledge of the properties of the materials, and of the peculiarities of the structure, especially in terms of alloy contents and layer thicknesses, is essential to realize devices operating at the desired specifications. In the case of

* Corresponding author.
E-mail address: miguel.montes@upm.es (M. Montes Bajo).
[1] Presently at the Institute for Quantum Electronics, ETH Zürich, CH-8093 Zürich, Switzerland.
[2] Presently at Université Versailles St Quentin/Paris Saclay. Groupe d'Etude de la Matière Condensée (Gemac), France.

https://doi.org/10.1016/j.apsusc.2021.150816
Received 9 June 2021; Received in revised form 22 July 2021; Accepted 30 July 2021
Available online 2 August 2021

ZnO/(Zn,Mg)O QWs precise knowledge of the QW and barrier thicknesses on the one hand, and of the potential barrier height (via Mg content) on the other is key to tune the transition energy between adjacent QWs to the optical phonon energy of the constituent materials in QCLs or to adjust the properties of ZnO-based hyperbolic metamaterials [15], to name a few applications.

In this work we report the use of the interface phonon-polariton resonances in ZnO/(Zn,Mg)O MQWs to determine the Mg content in the QW barriers. The modes are observed by IR reflectance spectroscopy and analyzed by a dielectric function model, and we take advantage of the fact that the high-energy LO phonon frequency of (Zn,Mg)O increases linearly and monotonically with Mg content at an approximate rate of 1.5 cm^{-1} per percentage of Mg [13].

The results on this work have strong practical implications for researchers working in ZnO-based devices since they show a way to monitor the precise composition of the layers of actual device structures after their growth. To obtain stacks of layers of the desired composition one usually relies on earlier calibrations made with thick test layers grown under specific conditions on which the alloy composition is determined by techniques such as photoluminescence, cathodoluminescence, energy dispersive X-ray spectroscopy, or secondary ion mass spectrometry. Thus, a one-to-one relationship between growth conditions and alloy composition *in test layers* can be obtained. However, when growing the actual device structures, the growers can only assume that the *a priori* obtained recipes are reproducible in the growth of the thin multilayers of the devices if they want to achieve the desired results and sometimes the reproducibility is not that good. Also, if one would like to verify the actual compositions of the finished structures, it is often impossible to assess due to the small amount of material involved and the complexity of the structures themselves, or it is difficult, costly, and involves destructive techniques. The advantage of using the interface phonon–polariton resonances to determine the Mg content of very thin (thickness below 15 nm in this work) semiconductor heterostructures by purely optical means lies on the fact that the measurements can be quickly done on the actual device structures avoiding the need to rely on test layers or the use of invasive/destructive techniques. We believe these results can be translated to other materials systems such as GaN- and GaAs-based devices.

2. Methods

A series of ZnO/(Zn,Mg)O MQW structures with nominal Mg contents ranging from 22 to 41 % is analyzed using the proposed method. Details on the structures are given in Table 1 and a schematic of the general structure of the samples is shown in Fig. 1. The QWs are n-doped

Table 1
Description of the samples employed in this work. L_{QW} and L_b are the QW and barrier thicknesses, respectively. In samples QWIP1 and QWIP2 the MQW structure is sandwiched between two thick (around 150 nm) ZnO layers Ga-doped 1×10^{19} and 3×10^{19} cm^{-3}, respectively.

Sample Name	Nominal Mg content (%)	L_{QW} (nm)	L_b (nm)	Number of QW periods	(Zn,Mg)O buffer thickness (nm)	QW doping (cm^{-3})
A	22	3	5	20	65	1×10^{20}
B	30	4	10	15	50	5×10^{19}
C	30	3	15	15	50	1×10^{19}
D	30	4	5	20	50	3.5×10^{19}
E	34	4	10	10	100	9×10^{19}
F	41	2.5	5	20	50	UID
QWIP1	18	2.5	10	20	None	1.5×10^{19}
QWIP2	30	2.7	10	15	None	3×10^{19}

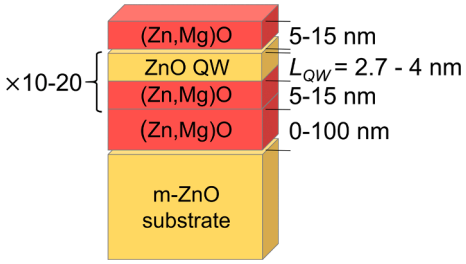

Fig. 1. Schematic of the samples employed in this work. Details on the specific thickness of each layer for each sample are given in Table 1.

with Ga at different levels. All the samples are grown by molecular beam epitaxy on non-polar, *m*-plane ZnO substrates. Samples A to F feature a 50 to 100 nm-thick (Zn,Mg)O buffer layer with the same nominal Mg content as the barriers in the MQWs. This buffer layer permits the measurement of the Mg content using catholodoluminescence (CL) spectroscopy as in [16]. The values obtained by CL are used in this work to calibrate the Mg content obtained from the analysis of the interface phonon-polariton modes. Two additional samples (QWIP1 and QWIP2) featuring the structure of quantum well infrared photodetectors (QWIPs) (i.e. the IR absorbing MQWs are sandwiched between two thicker, Ga-doped ZnO contact layers) are included. These samples serve a twofold purpose. First, to demonstrate that interface phonon-polaritons corresponding to the (Zn,Mg)O barriers are visible in actual device structures even though they are sandwiched between relatively thick Ga-doped ZnO contact layers. Second, that the modes are visible even in the absence of (Zn,Mg)O buffer layers or whenever the (Zn,Mg)O layers are buried inside the device structure.

Reflectance spectra are measured from all the samples at 30° angle of incidence of the *p*-polarized incident light in a Fourier transform infrared spectrometer (FTIR). The polarization of the incoming light is set using a KRS-5 holographic wire grid polarizer. The samples are grown on *m*-plane substrates (i.e. the *c*-axis is contained in the plane of the sample), therefore we choose the orientation of the *c*-axis so it lies perpendicular to the plane of incidence. Thus, $\boldsymbol{E} \perp c$ always and only the E_1 transverse phonon modes of the wurtzite structure (i.e. lattice vibrations perpendicular to the *c*-axis) are excited by the infrared light [13], simplifying the analysis of the spectra.

The obtained spectra are fitted with a transfer matrix model where all the constituent layers of the samples are modelled with a dielectric function accounting for the interaction of the light with the lattice and also the free electrons in case the layers are doped [4].

The (Zn,Mg)O layers are thus modelled with a dielectric function

$$\varepsilon_{(Zn,Mg)O} = \varepsilon_{\infty}^{(Zn,Mg)O} \prod_{k=1}^{2} \frac{\omega_{LO,k}^2 - \omega^2 - i\gamma_{LO,k}\omega}{\omega_{TO,k}^2 - \omega^2 - i\gamma_{TO,k}\omega}, \quad (1)$$

where $k = 1,2$ stands for the two phonon modes of (Zn,Mg)O for $\boldsymbol{E} \perp c$ [2]. $\varepsilon_{\infty}^{(Zn,Mg)O}$ is the high-frequency dielectric constant, $\omega_{LO,k}$ and $\omega_{TO,k}$ are the LO and TO phonon frequencies of the *k*-th mode, and $\gamma_{LO,k}$ and $\gamma_{TO,k}$ are broadenings of the *k*-th LO and TO phonon mode.

Intersubband transitions in doped QWs are only visible when the electric field of the light wave has a component perpendicular to the QWs [4]. To account for this, the dielectric function of the QWs is usually anisotropic, featuring the intersubband transition term only in the off-plane component. In this work, and in order to simplify the analysis, this anisotropy in the dielectric function has been neglected because the intersubband transitions lie far from the region where the interface phonon-polariton modes appear in the reflectance spectra and an isotropic dielectric function for the ZnO QWs including a phonon interaction term and a plasma interaction term is enough to reproduce well the experimental results in the range of interest in this work:

$$\varepsilon_{ZnO}(\omega) = \varepsilon_{\infty}^{ZnO}\frac{\omega_{LO}^2 - \omega^2 - i\omega\gamma_{LO}}{\omega_{TO}^2 - \omega^2 - i\omega\gamma_{TO}} - \frac{\omega_P^2}{\omega^2 + i\omega\gamma_P}. \quad (2)$$

The first term in (2) accounts for the interaction of light and phonons, analogously to (1). Here $\varepsilon_{\infty}^{ZnO}$ is the high-frequency dielectric constant of ZnO, and ω_{LO}, γ_{LO} and ω_{TO}, γ_{TO} are the frequencies and broadenings of the LO and TO phonon modes, respectively. The plasma frequency of the electrons in the QW is given by $\omega_P^2 = ne^2/\varepsilon_0 m^*$, with n the electron concentration in the QW, e the electron charge, ε_0 the permittivity of vacuum, and m^* the electron effective mass.

3. Results and discussion

Fig. 2 shows representative reflectance spectra of ZnO/(Zn,Mg)O QWs taken under *p*-polarization of the incident light. Two sharp dips appear in the reflectance spectra located at frequencies close to the LO phonon frequencies of ZnO (590 cm^{-1}) and (Zn,Mg)O (640–680 cm^{-1}, depending on the Mg content). These two features correspond to the interface phonon-polaritons at the interfaces between ZnO and (Zn,Mg)O layers.

Fig. 2(a) shows the shift to higher frequencies of the reflectance dip around 650 cm^{-1} when the nominal Mg content in the barrier layers is increased from 30 to 34 %. This shift correlates with the increase in the LO phonon frequency of (Zn,Mg)O with Mg content, which verifies the attribution of this reflectance feature to an interface phonon-polariton related to an interface with (Zn,Mg)O on one side. Fig. 2(b) shows that even for identical nominal Mg contents the reflectance dip can experience a shift due to the doping of the QWs. In other words, the excitation of plasma oscillations in the QW results in a small but noticeable shift of the interface phonon-polaritons related to the phonon of the adjacent, undoped layer. The calculated reflectance spectra included in Fig. 2 reproduce very well even the smallest features and variations in the experimental spectra due to the changes in QW doping and barrier Mg content. Therefore we can be confident that the values of ω_{LO} we obtain reproduce well the actual values in the barrier layers.

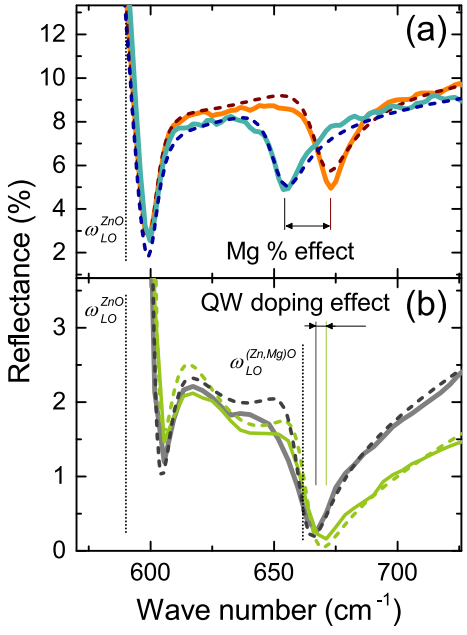

Fig. 2. (a) Reflectance spectra under *p*-polarization at 30° angle of incidence of two ZnO/(Zn,Mg)O MQW samples featuring nominal Mg contents of 30 (Sample B, orange) and 34 % (Sample E, blue). (b) Reflectance spectra under the same conditions from two samples identical to Sample C but different doping level in the QW (1×10^{18} cm^{-3}, green, vs 3×10^{19} cm^{-3}, grey). The thick curves are the experimental results and the thin, dotted curves are the fitted reflectance spectra calculated from the dielectric model. Vertical dotted lines indicate the values of ω_{LO} of the ZnO and (Zn,Mg)O layers employed in the calculation of the modelled spectra. (For interpretation of the references to colour in this figure legend, the reader is referred to the web version of this article.)

Due to its dispersive nature, the frequency at which the interface phonon-polariton is observed in the reflectance experiments depends on the angle of incidence (i.e. in-plane momentum of the incident light). This is illustrated with the reflectance spectra of Sample D in Fig. 3(a). Note that at all the angles of incidence that can be reached in this work (from 30° to 80°) the reflectance dip appears at an energy higher than $\omega_{LO}^{(Zn,Mg)O}$ (see also Fig. 2). This implies that simply taking the frequency of the reflectance dip as $\omega_{LO}^{(Zn,Mg)O}$ and then comparing it with the literature to obtain the Mg content can give rise to an inaccuracy that increases with the angle of incidence. Therefore, one needs to account for the dispersion relation of the interface phonon-polariton mode to correctly obtain the value of $\omega_{LO}^{(Zn,Mg)O}$ of the (Zn,Mg)O layers from the reflectance spectra. To do so, we fit the reflectance spectra of the entire stack of layers as described in the methods section for a 30° angle of incidence, and from this fit we obtain the angle-independent value of $\omega_{LO}^{(Zn,Mg)O}$. As an example of the reliability of the method, Fig. 3(b) shows the experimental value of the interface phonon-polariton frequency from the reflectance dip for Sample D as a function of the angle of incidence, together with the calculated dispersion relation. The

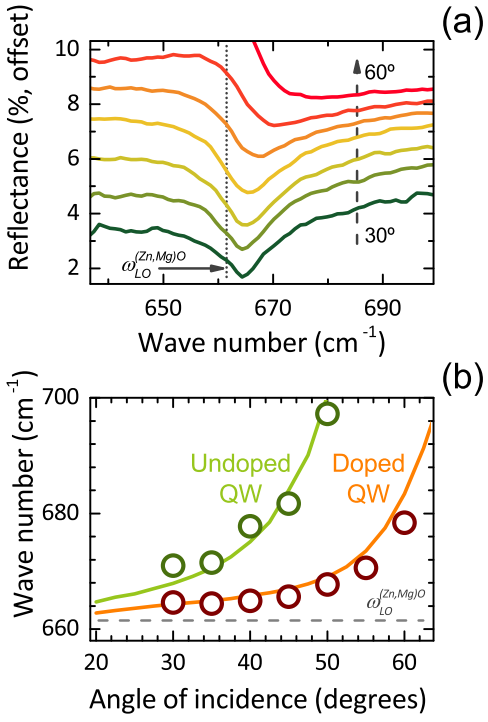

Fig. 3. (a) Reflectance spectra of Sample D for various angles of incidence of the light. The value of $\omega_{LO}^{(Zn,Mg)O}$, obtained from a fit to the experimental spectra at 30° angle of incidence, is indicated with a vertical dotted line. (b) Dispersion curve of the (Zn,Mg)O-related interface phonon-polariton of Sample D on the angle of incidence of the light, experimentally (orange circles) and from transfer matrix calculations (orange line). The calculations are performed using $\omega_{LO}^{(Zn,Mg)O}$ as obtained from the 30° reflectance spectrum. Note this value suffices to predict the frequency of the interface phonon-polariton at all angles with an accuracy better than 1 %. Results on the dispersion of the interface phonon-polariton for an equivalent, undoped sample are also included (the green line is the calculation, the circles are the experimental data). The grey, dashed line indicates the value of $\omega_{LO}^{(Zn,Mg)O}$ used in the transfer matrix calculations. (For interpretation of the references to colour in this figure legend, the reader is referred to the web version of this article.)

dispersion that would be observed if the QWs were not doped is also included.

The presence of electrons in the QW has another effect on the frequency of the reflectance dips. As shown before, the interface phonon-polariton at 650–680 cm^{-1} shifts to higher energies as the angle of incidence is increased (i.e. as the in-plane momentum of the incoming wave is increased, Fig. 3(a)). When there is no doping in the QW, the interface phonon-polariton mode frequency increases monotonously and unbounded with the angle of incidence. If the QW is doped, though, the interface phonon-polariton mode becomes only slightly dispersive, its frequency bounded below ~ 750 cm^{-1}. (Fig. 3(b)). The difference in frequency between doped and undoped structures is small for small angles of incidence, nevertheless the model accounts for it well.

Now, having shown that the method allows to obtain ω_{LO} in doped samples from one single reflectance spectrum, and that it reproduces well the spectra at other angles within a reasonable accuracy better than 1 %, we can illustrate its usefulness in obtaining the Mg content in the barrier layers of the samples. Fig. 4 shows the interface phonon-polariton at a fixed angle of incidence of the light of 30° for all the samples in this study. By fitting the reflectance spectra, ω_{LO} can be obtained for each sample and its value correlated to the Mg content using reported ω_{LO} vs Mg content values (see for example Bundesmann *et al.* [13]) or performing an additional calibration experiment, which is the approach we consider in this work.

In this sort of structures this content is usually calibrated via photoluminescence or cathodoluminescence (CL) measurements of a buffer layer placed underneath the active MQW structure. The need for a relatively thick buffer layer is because a certain amount of material has to be present so its luminescence can be detected. We have performed room-temperature CL measurements of the samples in this study and the results are shown in Fig. 5. Two peaks are apparent in the spectrum of each sample. One is located around 3.3 eV and corresponds to the recombination of electrons and holes in the ZnO quantum wells and substrate. The other one, the emission band ranging from around 3.7 to 4.0 eV, corresponds to electron-hole recombination at the (Zn,Mg)O buffer layers. The shift of this near-band edge (NBE) CL peak to higher energies as the Mg content is increased is apparent and reflects the increase in band gap of (Zn,Mg)O with increasing Mg [16].

From Fig. 5 we can extract the energy of the (Zn,Mg)O CL peak as a measure of the Mg content of the layers [16], and correlate it with the frequency of the (Zn,Mg)O LO phonon of the same sample extracted from the reflectance analysis. Fig. 6 shows there is an excellent linear correlation between these two magnitudes.

The values of the NBE CL peak energy of the (Zn,Mg)O layers can be converted to values of Mg content (top *x* axis in Fig. 6(a)) by interpolation from the data in [16], where the CL NBE peak energy of 1 μm-thick (Zn,Mg)O layers is correlated to the Mg content extracted from

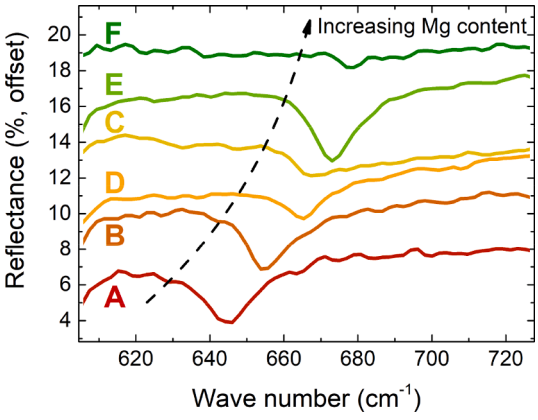

Fig. 4. Zoomed-in plot of the reflectance spectra around the dip related to the (Zn,Mg)O layers for all the samples featured in this study.

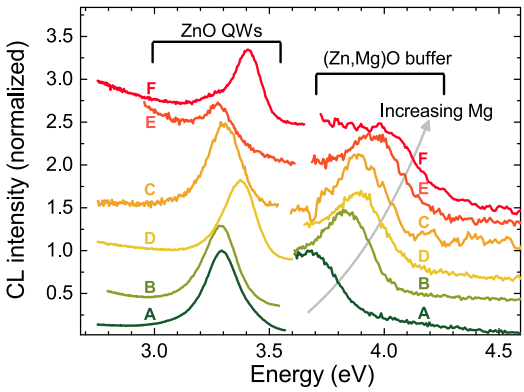

Fig. 5. Room-temperature CL spectra of samples A to F. The peaks corresponding to the near band edge emission of the ZnO QWs and the (Zn,Mg)O buffer layer have been normalized to unity and offset for clarity.

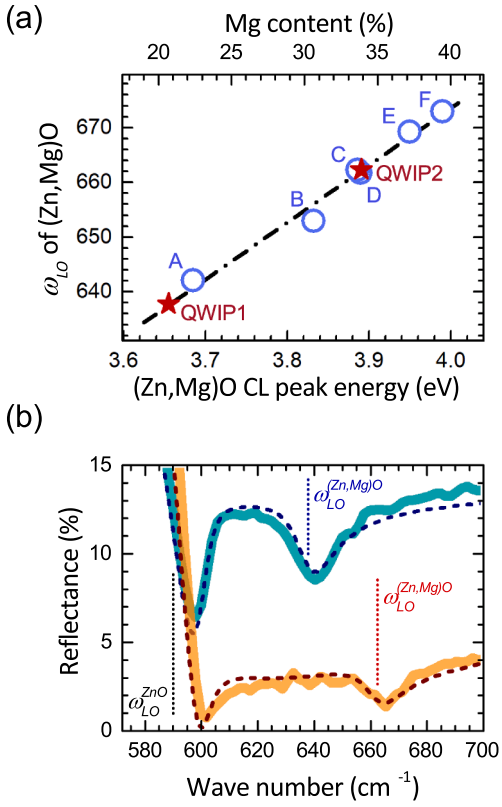

Fig. 6. (a) Correlation between the ω_{LO} of the (Zn,Mg)O layers of samples A to F, obtained from fits to the reflectance data, and their CL peak energy (circles). The dashed line is a linear fit to the data. The stars are the data points corresponding to samples QWIP1 and QWIP2. For these samples, ω_{LO} is known from the reflectance measurements and the dotted line is used to obtain the corresponding Mg content in actual device structures where there is no buffer layer. The correspondence between the bottom and top horizontal axes is made by interpolation from the data in [16]. (b) Experimental and fitted reflectance spectra at 30° and *p*-polarization of samples QWIP1 and QWIP2. Vertical dotted lines indicate the values of ω_{LO} from the model for ZnO and (Zn,Mg)O in each sample.

Rutherford backscattering experiments. The dotted line in Fig. 6(a) is a linear fit of the ω vs CL NBE peak energy data that can be now used as a calibrated curve to obtain the Mg content from ω_{LO}. The procedure would be as follows: From fits to the reflectance spectra, the frequency of ω_{LO} would be obtained; next one would go to Fig. 6(a) and, look for the Mg content that correspond to such ω_{LO} as stated by the dash-dotted

lined in the Figure.

To illustrate this procedure in actual device structures the *p*-polarized reflectance spectra at 30° of samples QWIP1 and QWIP2 are shown in Fig. 6(b) together with their respective fits. The values of ω_{LO} obtained from the fits are used in Fig. 6(a) to find the corresponding Mg content. As can be seen, the values of the Mg content obtained with this procedure are close to, but different than, the nominal ones (around 3% higher), which proves the usefulness of the approach described here. Fig. 6(b) also proves there is no need for a thick (Zn,Mg)O buffer layer for the interface phonon-polariton reflectance dip to be observable.

It is worth to spend some lines to discuss and estimate the uncertainty of this method. We focus on samples B, C, D, and QWIP2, which feature a nominal 30 % Mg content. Looking first at samples B, C, and D, we see a large difference in the obtained ω_{LO} (and therefore, Mg content), especially between Sample B on the one hand and samples C and D on the other. This difference correlates very well with the difference in NBE CL peak energy, which is our calibration technique, while staying in the linear trend of ω_{LO} vs NBE energy. This allows us to conclude that this different result is not a symptom of the uncertainty of the method, but rather that the samples indeed have different Mg content. The discrepancy in the actual values of Mg content might originate from the fact that Sample B was grown in a different system than C, D, and QWIP2.

Let's focus now on samples C and D. The difference in NBE energy between these two samples is of 4 meV ($\sim$ 0.1 % of the NBE energies). This, translates into a Mg content difference of approximately 0.2 %. Therefore, by our calibration method, we can conclude this two samples have the same Mg content within 0.2 %.

The difference in ω_{LO} observed between C and D is 0.6 cm^{-1} (that is, $\sim$ 0.1 % of the ω_{LO} values). So, the measurement we use for calibration yields roughly the same discrepancy than the optical method we propose. Therefore, we take this as an upper bound for the precision of the proposed method. A maximum uncertainty of 0.1 % in ω_{LO}, by the linear fit of Fig. 5(a), would translate into an uncertainty of less than 0.5 % in the determination of the Mg content.

As a final remark, QWIP2, whose nominal Mg content is also 30 %, is measured by our method to have 33.9 % Mg content. The measured value is within 0.3 % of the measured values of C and D, consistent with what was stated above.

4. Conclusions

The occurrence of interface phonon-polariton modes in the *p*-polarized, oblique incidence reflectance spectra of ZnO/(Zn,Mg)O MQWs was observed and their relation to LO phonons in the (Zn,Mg)O barrier layers was established. The value of $\omega_{LO}^{(Zn,Mg)O}$ of the barriers was obtained from fits to the reflectance spectra using dielectric function models. An application of the observations is shown by determining the Mg content in the thin barriers. The experimental reflectance is compared to transfer matrix dielectric function models to account for the dependence of the interface phonon-polariton modes on the angle of incidence and the electron concentration in the QW. The $\omega_{LO}^{(Zn,Mg)O}$ thus obtained is then correlated to the CL energy of the buffer layers of the samples for calibration purposes, which allows to obtain the actual Mg content in the structures. Finally, the applicability of this method is demonstrated in actual QWIP device structures where there is no buffer layer.

CRediT authorship contribution statement

M. Montes Bajo: Conceptualization, Investigation, Methodology, Visualization, Writing – original draft. **J. Tamayo-Arriola:** Investigation, Visualization, Writing – original draft. **N. Le Biavan:** Investigation, Resources, Writing – review & editing. **E. Martínez Castellano:** Writing – review & editing, Visualization. **D. Lefebvre:** Resources, Writing – review & editing. **M. Hugues:** Resources, Writing – review & editing. **J.-M. Chauveau:** Resources, Investigation, Funding acquisition, Project administration, Writing - review & editing. **A. Hierro:** Conceptualization, Funding acquisition, Supervision, Visualization, Writing – original draft.

Declaration of Competing Interest

The authors declare that they have no known competing financial interests or personal relationships that could have appeared to influence the work reported in this paper.

Acknowledgements

This work was funded by the Spanish Ministry of Economy and Competitiveness (MINECO) through Project TEC2017-85912-C2-1-R, and from the European Union's Horizon 2020 Research and Innovation Program under grant agreement No. 665107 (project ZOTERAC).

References

[1] A. Tsukazaki, A. Ohtomo, T. Kita, Y. Ohno, H. Ohno, M. Kawasaki, Quantum Hall Effect in Polar Oxide Heterostructures, Science 315 (5817) (2007) 1388–1391.
[2] A. Tsukazaki, S. Akasaka, K. Nakahara, Y. Ohno, H. Ohno, D. Maryenko, A. Ohtomo, M. Kawasaki, Observation of the fractional quantum Hall effect in an oxide, Nat. Mater. 9 (11) (2010) 889–893, https://doi.org/10.1038/nmat2874.
[3] J. Falson, D. Maryenko, B. Friess, D. Zhang, Y. Kozuka, A. Tsukazaki, J.H. Smet, M. Kawasaki, Even-denominator fractional quantum Hall physics in ZnO, Nat. Phys. 11 (4) (2015) 347–351, https://doi.org/10.1038/nphys3259.
[4] M. Montes Bajo, J. Tamayo-Arriola, M. Hugues, J.M. Ulloa, N. Le Biavan, R. Peretti, F.H. Julien, J. Faist, J.M. Chauveau, A. Hierro, Multisubband Plasmons in Doped ZnO Quantum Wells, Phys. Rev. Appl. 10 (2018), 024005, https://doi.org/10.1103/PhysRevApplied.10.024005.
[5] E. Fortunato, D. Ginley, H. Hosono, D.C. Paine, Transparent Conducting Oxides for Photovoltaics, MRS Bull. 32 (3) (2007) 242–247, https://doi.org/10.1557/mrs2007.29.
[6] G.V. Naik, J. Liu, A.V. Kildishev, V.M. Shalaev, A. Boltasseva, Demonstration of Al: ZnO as a plasmonic component for near-infrared metamaterials, PNAS. 109 (2012) 8834–8838.
[7] G. Tabares, A. Hierro, B. Vinter, J.-M. Chauveau, Polarization-sensitive Schottky photodiodes based on a-plane ZnO/ZnMgO multiple quantum-wells, Appl. Phys. Lett. 99 (7) (2011) 071108, https://doi.org/10.1063/1.3624924.
[8] F. Rahman, Zinc oxide light-emitting diodes: a review, Opt. Eng. 58 (01) (2019) 1, https://doi.org/10.1117/1.OE.58.1.010901.
[9] M. Belmoubarik, K. Ohtani, H. Ohno, Intersubband transitions in ZnO multiple quantum wells, Appl. Phys. Lett. 92 (19) (2008) 191906, https://doi.org/10.1063/1.2926673.
[10] A. Jollivet, B. Hinkov, S. Pirotta, H. Hoang, S. Derelle, J. Jaeck, M. Tchernycheva, R. Colombelli, A. Bousseksou, M. Hugues, N. Le Biavan, J. Tamayo-Arriola, M. Montes Bajo, L. Rigutti, A. Hierro, G. Strasser, J.-M. Chauveau, F.H. Julien, Short infrared wavelength quantum cascade detectors based on m-plane ZnO/ZnMgO quantum wells, Appl. Phys. Lett. 113 (25) (2018) 251104, https://doi.org/10.1063/1.5058120.
[11] N. Le Biavan, M. Hugues, M. Montes Bajo, J. Tamayo-Arriola, A. Jollivet, D. Lefebvre, Y. Cordier, B. Vinter, F.-H. Julien, A. Hierro, J.-M. Chauveau, Homoepitaxy of non-polar ZnO/(Zn, Mg)O multi-quantum wells: From a precise growth control to the observation of intersubband transitions, Appl. Phys. Lett. 111 (23) (2017) 231903, https://doi.org/10.1063/1.5003146.
[12] B. Meng, B. Hinkov, N.M. Le Biavan, H.T. Hoang, D. Lefebvre, M. Hugues, D. Stark, M. Franckié, A. Torres-Pardo, J. Tamayo-Arriola, M. Montes Bajo, A. Hierro, G. Strasser, J. Faist, J.M. Chauveau, Terahertz Intersubband Electroluminescence from Nonpolar m-Plane ZnO Quantum Cascade Structures, ACS Photonics. 8 (1) (2021) 343–349, https://doi.org/10.1021/acsphotonics.0c0164110.1021/acsphotonics.0c01641.s001.
[13] C. Bundesmann, A. Rahm, M. Lorenz, M. Grundmann, M. Schubert, Infrared optical properties of MgxZn1−xO thin films (0⩽x⩽1): Long-wavelength optical phonons and dielectric constants, J. Appl. Phys. 99 (11) (2006) 113504, https://doi.org/10.1063/1.2200447.
[14] E. Bellotti, K. Driscoll, T.D. Moustakas, R. Paiella, Monte Carlo simulation of terahertz quantum cascade laser structures based on wide-bandgap semiconductors, J. Appl. Phys. 105 (11) (2009) 113103, https://doi.org/10.1063/1.3137203.
[15] A. Hierro, M. Montes Bajo, M. Ferraro, J. Tamayo-Arriola, N. Le Biavan, M. Hugues, J.M. Ulloa, M. Giudici, J.M. Chauveau, P. Genevet, Optical Phase Transition in Semiconductor Quantum Metamaterials, Phys. Rev. Lett. 123 (2019), 117401, https://doi.org/10.1103/PhysRevLett.123.117401.
[16] G.M. Foster, J. Perkins, M. Myer, S. Mehra, J.M. Chauveau, A. Hierro, A. Redondo-Cubero, W. Windl, L.J. Brillson, Native point defect energies, densities, and electrostatic repulsion across (Mg, Zn)O alloys, Phys. Status Solidi A. 212 (7) (2015) 1448–1454, https://doi.org/10.1002/pssa:201532285.